Atmospheric
Chemistry
and Physics
Discussions

Open Access

Injection of mineral dust into the free troposphere during fire events observed with polarization lidar at Limassol, Cyprus

A. Nisantzi[1], R. E. Mamouri[1], A. Ansmann[2], and D. Hadjimitsis[1]

[1]Cyprus University of Technology, Dep. of Civil Engineering and Geomatics, Limassol, Cyprus
[2]Leibniz Institute for Tropospheric Research, Leipzig, Germany

Correspondence to: A. Nisantzi (argyro.nisantzi@cut.ac.cy)

Discussion Paper | Discussion Paper | Discussion Paper | Discussion Paper |

ACPD

14, 17299–17329, 2014

Soil dust in fire smoke plumes

A. Nisantzi et al.

Title Page

Abstract	Introduction
Conclusions	References
Tables	Figures

|◄ ►|

◄ ►

Back Close

Full Screen / Esc

Printer-friendly Version

Interactive Discussion

Title Page

Abstract | Introduction

Conclusions | References

Tables | Figures

◄◄ | ►►

◄ | ►

Back | Close

Full Screen / Esc

Printer-friendly Version

Interactive Discussion

Abstract

Four-year observations (2010–2014) with EARLINET polarization lidar and AERONET sun/sky photometer at Limassol (34.7° N, 33° E), Cyprus, were used to study the soil dust content in lofted fire smoke plumes advected from Turkey. This first systematic attempt to characterize less than 3 days old smoke plumes in terms of particle depolarization contributes to the more general effort to properly describe the life cycle of free-tropospheric smoke–dust mixtures from the emission event to phases of long-range transport (> 4 days after emission). We found significant differences in the particle depolarization ratio (PDR) with values from 9–18 % in lofted aerosol layers when Turkish fires contributed to the aerosol burden and of 3–13 % when Turkish fires were absent. High Ångström exponents of 1.4–2.2 during all these events with lofted smoke layers, occuring between 1 and 3 km height, suggest the absence of a pronounced particle coarse mode. When plotted vs. the travel time (spatial distance between Limassol and last fire area), PDR decreased strongly from initial values around 16–18 % (one day travel) to 4–8 % after 4 days of travel caused by deposition processes. This behavior was found to be in close agreement with the literature. Computation of particle extinction coefficient and mass concentrations, separately for fine-mode dust, coarse-mode dust, and non-dust aerosol components show extinction-related dust fractions of the order of 10 % (for PDR = 4 %, travel times > 4 days) and 50 % (PDR = 15 %, one day travel time) and mass-related dust fractions of 25 % (PDR = 4 %) to 80 % (PDR = 15 %). Biomass burning should be considered as another source of free tropospheric soil dust.

1 Introduction

Biomass burning smoke affects air quality, visibility, and climate directly and indirectly. Hot fire smoke plumes easily reach the free troposphere (FT) and can be transported from continent to continent within one week (Fiebig et al., 2002; Mattis et al., 2003;

Soil dust in fire smoke plumes

A. Nisantzi et al.

Murayama et al., 2004; Müller et al., 2005; Petzold et al., 2007; Ansmann et al., 2009; Baars et al., 2011) and around the globe within 2–3 weeks (Damoah et al., 2004). Fire smoke must be regarded as an important source of the free-tropospheric background aerosol. It is well known that the strong winds inside the combustion zones can raise

5　considerable amounts of soil particles into the atmosphere (Palmer, 1981; Gaudichet et al., 1995; Maenhaut et al., 1996) which are preferable cloud condensation and ice nuclei (Pratt et al., 2011). Fires around the world may thus also be significant sources of FT dust particles. These plumes partly reach the upper troposphere (Mattis et al., 2008; Dahlkötter et al., 2014).

10　For an adequate consideration of fire-related dust particles in atmospheric models, it is desirable to improve our knowledge about the lifecycle of fire smoke plumes from the emission and regional transport during the first several days up to the long-range and intercontinental transport and corresponding travel times of 7–20 days after emission. From ground-based in situ aerosol field studies close to fires, we know that soil dust

15　particles form a pronounced coarse mode in the begin. According to Gaudichet et al. (1995) and Maenhaut et al. (1996) 75–99 % of the coarse particles were found to be dust in smoke of flaming African savanna fires. In contrast, airborne in-situ observations of fire smoke plumes after long-range transport of 4–6 days indicate that super micrometer particles (coarse-mode particles) are almost absent in the aged smoke plumes, but

20　that the accumulation mode is enhanced and shifted to mode diameters of 200–400 nm compared to smoke–free background aerosol observations (Fiebig et al., 2002; Petzold et al., 2007; Dahlkötter et al., 2014). Particle depolarization ratios of 6–8 % and sometimes up to 15 % in North American fire smoke after long range transport observed with polarization lidars (Fiebig et al., 2002; Murayama et al., 2004), point to fine-mode

25　dust particles contributions of about 5–40 % to the observed particle optical properties of the aged smoke layers. Polarization lidar observations of the particle linear depolarization ratio allow us to separate fine-mode and coarse-mode dust and distinguish dust from non-dust aerosol contributions to the measured particle mass concentration, optical depth, and extinction coefficients (Mamouri and Ansmann, 2014). Only

irregularly shaped partices such as mineral dust particles (soil, road, and desert dust) cause strong depolarization of emitted linearly polarized laser light, whereas spherical or almost spherical particles such as anthropogenic haze, biomass-burning smoke, and marine particles do not produce strong depolarization of backscattered light (Groß

5   et al., 2011, 2013; Ansmann et al., 2011, 2012).

To better characterize free-tropospheric fire smoke plumes and mixtures of dust and smoke as well as changes in the microphysical and optical properties of these mixed aerosol layers with travel time, lidar measurements of the particle depolarization ratio in fires smoke plumes especially during the first 3 days after emisson are required.

10   A first systematic attempt to fill this gap is undertaken in this paper. We analyzed polarization lidar observations performed at the EARLINET site of Limassol, Cyprus, from April 2010 to February 2014. These results are presented in Sect. 3. In our study, we concentrated on air masses advected from Turkey and regions further north of the Black Sea area during the main burning seasons (summer half years). We sepa-

15   rated cases with strong impact of smoke events (occuring over Turkey during 1–3 days before arrival at Limassol) from observation with more background–like aerosol signatures (not influenced by Turkish fire smoke). We found significant differences in the depolarization characteristics of the backscattered layer light. The particle depolarization ratio (the defintion is given in the Sect. 2) was typically 10–15 % when Turkish

20   fires contributed to the aerosol burden in the free troposphere and considerably lower with values of 3–8 % when fires over Turkey were absent while the air masses crossed this country. AERONET photometer observations showed high Ångström exponents (mainly from 1.4–2.0) during all these events with lofted smoke layers suggesting the absence of a pronounced particle coarse mode. Depolarization ratios of 10–15 % then

25   point to fine-mode dust contributions of the order of 50 % to the observed optical particle properties as will be discussed in Sect. 3.

The paper is organized as follows: In Sect. 2, the lidar and photometer instruments as well as the lidar data analysis are briefly described. Section 3 presents observational case studies and statictical results of our aerosol observations, and integrates

Soil dust in fire smoke plumes

A. Nisantzi et al.

Title Page

Abstract	Introduction
Conclusions	References
Tables	Figures

⏮   ⏭

◀   ▶

Back   Close

Full Screen / Esc

Printer-friendly Version

Interactive Discussion

the findings into the broader context of published lidar observations of aged smoke–dust plumes. A summary and concluding remarks are given in Sect. 4.

2   Instrumentation and data analysis tools

2.1   EARLINET polarization lidar

The lidar station of the Cyprus University of Technology (CUT) at Limassol (34.7° N, 33° E, 50 m a.s.l.) (Mamouri et al., 2013) is member of the Europaen Aerosol Research Lidar Network (EARLINET) (Pappalardo et al., 2014). The site is located about 150 km south of Turkey and 400 km west of Syria. The lidar transmits linearly polarized laser pulses at 532 nm and detects the parallel- and cross-polarized signal components at this wavelength. From the calibrated ratio of the cross-to-parallel-polarized lidar signals the volume linear depolarization ratio can directly be determined (Freudenthaler et al., 2009). Calibration of the polarization channels is performed by rotating the box with the polarization sensitive channels following the methodology of Freudenthaler et al. (2009). The transmission properties of the receiver (for parallel and perpendicularly polarized light) required for an accurate determination of the particle linear depolarization ratio are known from measurements.

The full overlap of the laser beam with the receiver field of view of the 20 cm Cassegrain telescope is obtained at heights around 300 m a.s.l. (Mamouri et al., 2013). The measured volume depolarization ratio is reliable to about 50 m above ground. Overlap effects widely cancel out here because the depolarization ratios are calculated from signal ratios.

Our study presented in Sect. 3 is based on height profiles of the particle backscatter coefficient and the particle depolarization ratio at 532 nm. The determination of the particle backscatter coefficient is described in detail by Mamouri et al. (2013). The particle depolarization ratio is computed from the volume depolarization ratio by means of the determined particle backscatter coefficient (Freudenthaler et al., 2009). Uncertainties

in the retrieval products are discussed by Mamouri et al. (2013) and are typically of the order of 10 %.

In the retrieval of the particle depolarization ratio, the Rayleigh depolarization ratio, i.e., the depolarization ratio for particle–free air must be known. The Rayleigh depolarization ratio is estimated from the volume depolarization ratio during clear days in aerosol–free air. Figure 1 presents two examples. Although the shown volume linear depolarization ratio is noisy at heights above the main aerosol layers reaching up to about 2–3 km height one can see that the volume depolarization ratio assumes values around 1 % at heights above 4 km. The volume depolarization is equal to the depolarization ratio for pure Rayleigh backscattering (in cases with negligible particle backscattering). In the data analysis, discussed in Sect. 3, we used a fixed Rayleigh depolarization ratio of 1.3 % for all measurement cases. The uncertainty introduced by a wrong Rayleigh value of ±1 % is of the order of 1–2 % in the particle depolarization ratio.

Figure 1 also shows that the volume depolarization ratio in pronounced aerosol layers can be as low as about 2 % in cases with westerly winds (right panel) when maritime particles and aged anthropogenic haze from western, southern, and central Europe dominate the aerosol conditions over the eastern Mediterranean. Values around 2–3 % are typical for maritime particles (Groß et al., 2011, 2013). Minor contributions of road dust, soil dust emitted around Limassol, and dried maritime particles to the measured depolarization ratios must always be taken into account when studying lidar observations at Limassol.

Recently, a new polarization-lidar-based method was introduced by Mamouri and Ansmann (2014) that allows us to separate spherical (marine and continental fine-mode and marine coarse-mode particles), which cause particle depolarization ratios < 3 %, fine-mode dust particles causing particle depolarization ratios around 16 % (Sakai et al., 2010), and coarse-mode dust particles causing particle depolarization ratios around 39 % (Sakai et al., 2010). The fine mode includes all particles with radii < 500 nm. We used the new technique to estimate the contribution of fine-mode

Soil dust in fire smoke plumes

A. Nisantzi et al.

and coarse-mode dust to the mass concentrations and particle extinction coefficients in the detected smoke–dust plumes in Sect. 3.

As described by Mamouri and Ansmann (2014), a two-step approach is applied to the measured 532 nm backscatter-coefficient profiles. In our study, we explicitly assume that free-tropospheric spherical particles cause depolarization ratios of 1 % (in the absence of any marine particle contribution in the lofted continental aerosol plumes), that the fine mode aerosol mixture of smoke and dust causes a particle depolarization ratio of 8 % (assuming a mixture of roughly 50 % smoke and 50 % dust), and that, as mentioned, the coarse-mode dust particles cause a depolarization ratio of 39 %. According to the error discussions by Mamouri et al. (2013) and Mamouri and Ansmann (2014) the overall uncertainty in the separation of the backscatter and extinction coefficients for the different aerosol types is of the order of 20–40 %, and the uncertainty in the retrieved mass concentration profiles may be of the order of 50 %.

2.2 AERONET sun/sky photometer

The lidar is collocated with a sun/sky photometer of the Aerosol Robotic Network (AERONET, CUT-TEPAK site, Limassol, Cyprus, http://aeronet.gsfc.nasa.gov) (Holben et al., 1998). The CUT AERONET photometer measures the aerosol optical thickness (AOT) at eight wavelengths from 339 to 1638 nm. From the spectral AOT distribution, the Ångström exponent AE (Ångström, 1964), and the fine mode fraction FMF (fraction of fine-mode AOT to total AOT) (O'Neill et al., 2003) are retrieved. AOT errors are of the order of 0.01–0.02 in the absence of unfiltered cloud contamination (Chew et al., 2012).

2.3 Combined lidar/photometer data analysis

Mamouri et al. (2013) provides a detailed description of the lidar data analysis to obtain height profiles of particle backscatter and extinction coefficients at 532 nm which are in good agreement with the column-integrated photometer observations of AOT. In

Title Page

Abstract | Introduction

Conclusions | References

Tables | Figures

|◄ | ►|

◄ | ►

Back | Close

Full Screen / Esc

Printer-friendly Version

Interactive Discussion

this approach, the particle depolarization ratio is used to distinguish dust and non-dust contributions to the particle optical properties. Besides height profiles of the particle optical properties, essential products are the derived extinction-to-backscatter ratios (lidar ratios) for the entire tropospheric column S_{col}, for the free troposphere S_{FT}, and lidar ratios for dust $S_{FT,D}$ in the free troposphere. Climatological values (obtained from the long–term observations at Limassol) for the lidar ratio S_{PBL} of 20–35 sr in the planetary boundary layer (PBL), i.e., for the lowermost 300–400 m of the tropospheric column, where the overlap of the laser beam with the receiver field-of-view is incomplete, and for the non-dust free-tropospheric lidar ratio $S_{FT,S}$ of 40–60 sr are required in this retrieval as assumed input. Index S denotes fine-mode spherical particles in the free troposphere such as fire smoke and anthropogenic haze particles.

2.4 HYSPLIT backward trajectories

In order to investigate the influence of fire activities on the observed optical properties of the lofted aerosol plumes crossing Cyprus we studied the air mass transport by means of backward trajectory analysis. The calculations were performed with the HYSPLIT (HYbrid Single-Particle Lagrangian Integrated Trajectory) Model. Access is provided via the NOAA ARL READY Website (http://www.arl.noaa.gov/HYSPLIT.php). HYSPLIT is described in detail in Draxler and Hess (1997, 1998), and Draxler (1999).

2.5 MODIS fire products

In order to identify the areas where biomass burning aerosols were generated, MODIS (Moderate Resolution Imaging Spectroradiometer) active fire products were used (Flynn et al., 2002; Giglio et al., 2003). MODIS comprises a multi-spectral sensor with 36 spectral bands and covers the wavelengths range from 0.4 to 14.2 µm. Single fires are detected with 1 km spatial resolution. MODIS is flown aboard the two NASA Earth Observing System (EOS) satellites Terra and Aqua. Both satellites are polar orbiting. Fires at the 1 km scale can be measured up to four times per day. The MODIS algo-

rithms (including the fire algorithm) are updated periodically, leading to different versions, which are used to generate a series of Collections of the data products. The latest (Collection 5) fire data were used in this study.

We show five-day fire spots, i.e., all spots detected within five days. Data from University of Hawaii (http://modis.higp.hawaii.edu/) are taken. These fire events are combined with four-day HYSPLIT backward trajectories in order to estimate the presence and age of smoke plumes detected with the EARLINET lidar.

3 Results

The focus of our study is the investigation of the potential of open fires (wild fires and controlled biomass burning) to trigger injection of soil dust into the free troposphere. Another goal was to concentrate on young smoke plumes (not older than 1–3 days). Therefore, we only consider measurement cases of air mass transport from northerly directions crossing Turkey. We observed 45 respective cases from April 2010 to February 2014. In 24 out of the 45 cases presented here, the backward trajectories together with the MODIS fire maps indicated that the measured lidar profiles were influenced by Turkish fire smoke.

We begin with two case studies. The measurement examples in Figs. 2 and 4 together with Figs. 3 and 5 (HYSPLIT backward trajectories and MODIS fire information) provide a contrasting impression of the differences in the observed particle depolarization ratios when no fires were observed by MODIS over Turkey (Fig. 2) and when several fires over central Turkey influenced the lidar measurements over Limassol significantly (Fig. 4). In the smoke-free case, the particle depolarization ratio was less than 10 % throughout the entire free troposphere from 500 m to 4 km height. The aerosol plume was well mixed. The moderately enhanced particle depolarization ratios (compared to low values of 1–3 % for haze pollution and fine-mode smoke) may indicate the influence of soil dust from arid regions, from remote deserts, and dust injected during

Title Page

Abstract   Introduction

Conclusions   References

Tables   Figures

◄   ►►

◄   ►

Back   Close

Full Screen / Esc

Printer-friendly Version

Interactive Discussion

fires at times 3–7 days before the arrival of the air masses at Limassol from areas north of the Black Sea.

The Ångström exponent of $AE_A = 1.67$ and fine mode fraction $FMF_A = 0.76$ from the AERONET observations indicate the dominance of fine mode particles throughout the entire troposphere. The particle optical depth of $AOT_A = 0.31$ and extinction-to-backscatter ratios S_{FT} around 35 sr in the free troposphere indicate a high aerosol load of a mixture of aged, less absorbing anthropogenic haze, fire smoke, and background aerosols from rural areas.

Figure 4 represents a measurement case with strong influence of Turkish fire smoke (see also Fig. 5). Again, a well mixed lofted layer of smoke and dust was found above 1 km height. The layer-mean particle depolarization ratio of almost 18 % is the highest depolarization value we observed during the 4 years of lidar measurements. However most of the dust seems to be again fine-mode dust because the Ångström exponent of $AE_A = 1.45$ and the fine mode fraction $FMF_A = 0.79$ are again comparably high. Lidar ratios S_{FT} in the free troposphere of around 50 sr point to a mixture of moderately absorbing smoke particles (60 sr) and less absorbing, non-spherical dust particles (35–45 sr).

Figure 6 provides an overview of the geometrical properties of all aerosol layers in the lower free troposphere observed during the four-year period from February 2010 to April 2014. Most layers were found between 1 and 3 km height with layer centers around 1.9–2 km height. On average, the smoke layers showed a vertical extent of 1.4–1.5 km.

Figure 7 presents the time series of derived layer-mean particle depolarization ratios. Most values were > 10 % when the air masses crossed fire areas over Turkey. For cases free of Turkish smoke we observed values from 3–13 %. Depolarization ratios below < 4 % may indicate dust–free conditions in the free troposphere.

An overview of the optical properties (range of values) of all layers for northerly air mass advection is presented in Fig. 8. Layers with comparably fresh fire smoke from Turkey (red symbols, depolarization values from 9–18 %) showed low backscatter coef-

ficients around $1 \pm 0.5 \, \text{Mm}^{-1} \, \text{sr}^{-1}$. Multiplication with a tyical lidar ratio of 40–50 sr yields smoke–dust layer particle extinction coefficients of the order of 25–75 Mm^{-1}. For the smoke-free cases, several large backscatter coefficients $> 3 \, \text{Mm}^{-1} \, \text{sr}^{-1}$ were observed which may indicate the influence of marine particles. Even during northerly airflows,

5   sea breeze effects at the south coast of Turkey and the north coast of Cyprus (including mountain-induced circulation effects over Cyprus) and corresponding injection of marine particles into the lowermost 1–2 km of the atmosphere can never be completely excluded when interpreting free-tropospheric lidar observations at Limassol. But as shown, these events are rare.

10   The 532 nm AOT for smoke–dust plumes was found to be in the range from 0.05–0.25. According to Mattis et al. (2003), Murayama et al. (2004) and Müller et al. (2005) AOT decreases to values of 0.02–0.05 after long-range transport of 4–15 days. Lidar ratios of the smoke–dust layers range from 25–60 sr, and indicate at all less absorbing aerosol layers (red symbols in Fig. 8, third panel). Low values of < 25 sr can be caused

15   by rural background aerosols (Hänel et al., 2012) as well as by marine particles (Groß et al., 2011). Ångström exponents for the entire tropospheric column from 1.4–2.2 indicate that the smoke–dust plumes mainly consisted of fine-mode particles (Aitken mode, accumulation mode). Coarse-mode dust particles were obviously removed quickly and efficiently. Similarly, fine mode fractions for the entire tropospheric column (including

20   the marine boundary layer and thus coarse marine particles) of 0.55–0.95 indicate the dominance of fine-mode particles in the lofted smoke–dust aerosol mixtures. Markham et al. (1997), O'Neill et al. (2002) and Müller et al. (2007) also reported Ångström exponents > 1.4 during fire smoke events (within the first 2–3 days after emission).

Figure 9 shows the dependence of the layer-mean particle depolarization ratio on

25   travel time (i.e., the spatial distance between Limassol and the last fire area upwind of the lidar site). The travel time is calculated from the HYSPLIT backward trajetories for the smoke layer centers. As can be seen, the depolarization ratio drops from 14–18 % (day 1) to about 5 % (day 4). Several literature values are shown in addition and corroborate the observed trend. Our fire smoke data (< 4 days old smoke) together with

Soil dust in fire smoke plumes

A. Nisantzi et al.

Full Screen / Esc

Printer-friendly Version

Interactive Discussion

literature values provide, for the first time, an impression how fast the depolarization ratio and thus the dust fraction decreases with time. Our data clearly fill an observational gap and contribute to the effort to properly describe the life cycle of free-tropospheric smoke–dust mixtures from the emission event to phases of long-range transport.

Assuming mean wind speeds of $5–10\,\mathrm{m\,s^{-1}}$ in the lower free troposphere over Turkey and areas north of Turkey, the air masses travelled 450–900 km per day. At greater heights wind speeds of $>15\,\mathrm{m\,s^{-1}}$ are typical so that smoke plumes may travel >1350 km per day (as is the case for the shown literature cases in Fig. 9).

The observed scatter in the data in Fig. 9 can be related to many reasons. First of all, there are uncertainties in the assignment of the fire events (after MODIS) to our lidar observations by using uncertain backward trajectories and fire information integrated over five days. Second, the soil characteristics and fire-induced dust injection efficiency may differ significantly from site to site, even for favorable arid regions such as Turkey. The literature values in Fig. 9 include Siberian as well North American biomass-burning smoke plumes. Third, free-tropospheric meteorological conditions can vary strongly along the transport path ways and thus also the aerosol mixing, diffusion, and deposition processes. Fourth, flaming fires as well as smoldering fires can occur. Flaming fires may be more efficient regarding the mobilization of surface soil dust. Fifth, some plumes observed with lidar may have been influenced by many (flaming and smoldering) fires, others by just one (flaming or smoldering) burning event. Sixth, it can also not be excluded that large, irregularly-shaped fire particles affected the lidar depolarization measurement, especially in very fresh smoke plumes. Finally, the nearby deserts in the Middle East and North Africa may have also contributed to the free tropospheric dust load.

In Figs. 10 and 11 two cases with high depolarization ratio in the smoke plume (PDR = 14 %, travel time < 2 days) and low depolarization ratio (PDR = 4.6 %, travel time of 4 days) are shown to quantify the range of dust contributions to the observed optical properties in the free tropospheric layer. The profiles of particle extinction coefficient were computed from the retrieved backscatter coefficients by using a lidar ratio

Soil dust in fire smoke plumes

A. Nisantzi et al.

Title Page

Abstract	Introduction
Conclusions	References
Tables	Figures

◄ | ►|

◄ | ►

Back | Close

Full Screen / Esc

Printer-friendly Version

Interactive Discussion

$S_{\text{FT,S}}$ of 45 sr for fine-mode spherical particles and the retrieved dust lidar ratios $S_{\text{FT,D}}$ were close to 30 sr in these specific two cases. As mentioned in Sect. 2, the retrieval is explained in detail by Mamouri et al. (2013) and Mamouri and Ansmann (2014).

On 25 August 2011 (Fig. 10), smoke layer mean extinction coefficients were 18 Mm^{-1} (fine-mode smoke), 10 Mm^{-1} (fine-mode dust), and 8 Mm^{-1} (coarse-mode dust). The dust fraction (DF) of particle extinction and optical depth was thus 50 %. The fine-mode fraction, i.e., the ratio of the sum of the AOTs of fine-mode dust and fine-mode spherical particles to the total AOT (at 500 nm) was 0.7 for the total tropospheric column (AERONET) and 0.77 in the FT on the basis of the lidar–derived profiles shown in Fig. 10.

On 25 June 2012 (Fig. 11) the FT aerosol layer was almost smoke free. The mean extinction coefficients in the lofted layer from 400–3000 m were 86.5 Mm^{-1} for spherical particles (probably mainly fine-mode urban haze) and 12.5 Mm^{-1} for fine-mode dust. The dust fraction was in this case DF$_{\text{L}}$ = 12 %. The fine-mode fraction after AERONET was 0.79, and 1 in the free troposphere according to the lidar extinction profiles in Fig. 11. Ångström exponents of 1.41 and 1.56 indicate the dominance of fine-mode particles in both cases.

In terms of particle mass concentration, the dust fraction in the mixed aerosol plumes is even higher. This is shown in Fig. 12. Mass concentrations were determined from the extinction coefficient profiles after Ansmann et al. (2012) and Mamouri and Ansmann (2014). In this estimation we used particle densities of 2.6 and 1.55 g cm^{-3} for mineral dust particles and non-dust fine-mode particles, respectively. For the required particle volume-to-extinction conversion factors (Ansmann et al., 2012) we applied values of 0.2×10^{-6} m, 0.3×10^{-6} m, and 0.8×10^{-6} m for fine-mode spherical particles, fine dust, and coarse dust, respectively.

As can be seen in Fig. 12, the layer mean particle mass concentrations were about 5.5 µg m^{-3} (fine-mode spherical smoke particles), 8 µg m^{-3} (fine-mode dust), and 16.5 µg m^{-3} (coarse-mode dust) for the smoke case observed on 25 August 2011. The dust fraction was about 80 % on this day. Even on 25 June 2012 (case with background-

level smoke and dust) the dust mass fraction was 25 % for the observed case with the low PDR = 4.6 %. We can conclude that dust mass fractions were of the order of 30–70 % in aged smoke-dust plumes observed over Limassol after travel times of 2–4 days. Fire smoke aerosol plumes in the free troposphere must be regarded as a non–negligible reservoir for dust and thus for cloud condensation and ice nuclei in the free troposphere.

4 Conclusions

Four-year observations (2010–2014) with EARLINET polarization lidar and AERONET sun/sky photometer at Limassol (34.7° N, 33° E), Cyprus, were used to study the soil dust content in lofted fire smoke plumes advected from Turkey. This first systematic attempt to characterize less than 3 days old smoke plumes in terms of particle depolarization filled an observational gap and contributes to the more general effort to properly describe the life cycle of free-tropospheric smoke–dust mixtures from the emission event to phases of long-range transport.

We found significant differences in PDR. PDR was 9–18 % in lofted Turkish smoke–dust–haze aerosol layers and considerably lower with values of 3–13 % when Turkish fires were not detected by MODIS. AERONET photometer observations showed high Ångström exponents (1.4–2.2) during all these events with lofted smoke layers suggesting the absence of a pronounced particle coarse mode. The lofted aerosol layers typically occurred between 1 and 3 km height. When plotted vs. the travel time (defined as the spatial distance between Limassol and last fires area), PDR decreased strongly from initial values around 16–18 % (1 day travel) to 4–8 % after 4 days of travel, in agreement with the literature. Computation of particle extinction coefficient and mass concentrations, separately for fine-mode dust, coarse-mode dust, and non-dust aerosol components shows extinction-related dust fractions of the order of 10 % (PDR = 4 %, after times of > 4 days) to 50 % (PDR = 15 %, after travel times of 1 day) and mass-related dust fractions of 25 % (PDR = 4 %) to 80 % (PDR = 15 %). Biomass burning in

arid regions must obviously be regarded as a significant source of soil dust that contributes to the background aerosol burden of the free troposphere.

Our study must however be regarded as a first step. More efforts of polarization lidar monitoring of fresh and aged smoke–dust plumes are required at very different places around the world to support our findings. The arid regions in the southeastern part of Europe and in the western part of Asia together with the deserts in the Middle East and Northern Africa may provide rather favorable conditions for dust injection into the atmosphere (free troposphere). Such almost optimum conditions may not be given at higher latitudes in the Northern Hemisphere as well as in large parts of the Southern Hemisphere.

References

Ångström, A.: The parameters of atmospheric turbidity, Tellus, 16, 64–75, 1964. 17305

Ansmann, A., Baars, H., Tesche, M., Müller, D., Althausen, D., Engelmann, R., Pauliquevis, T., and Artaxo, P.: Dust and smoke transport from Africa to South America: lidar profiling over Cape Verde and the Amazon rainforest, Geophys. Res. Lett., 36, L11802, doi:10.1029/2009GL037923, 2009. 17301

Ansmann, A., Tesche, M., Seifert, P., Groß, S., Freudenthaler, V., Apituley, A., Wilson, K. M., Serikov, I., Linné, H., Heinold, B., Hiebsch, A., Schnell, F., Schmidt, J., Mattis, I., Wandinger, U., and Wiegner, M.: Ash and fine-mode particle mass profiles from EARLINET-AERONET observations over central Europe after the eruptions of the Eyjafjallajökull volcano in 2010, J. Geophys. Res., 116, D00U02, doi:10.1029/2010JD015567, 2011. 17302

Ansmann, A., Seifert, P., Tesche, M., and Wandinger, U.: Profiling of fine and coarse particle mass: case studies of Saharan dust and Eyjafjallajökull/Grimsvötn volcanic plumes, Atmos. Chem. Phys., 12, 9399–9415, doi:10.5194/acp-12-9399-2012, 2012. 17302, 17311, 17329

Baars, H., Ansmann, A., Althausen, D., Engelmann, R., Artaxo, P., Pauliquevis, T., and Souza, R.: Further evidence for significant smoke transport from Africa to Amazonia, Geophys. Res. Lett., 38, L20802, doi:10.1029/2011GL049200, 2011. 17301

Chew, B. N., Campbell, J. R., Reid, J. S., Giles, D. M., Welton, E. J., Salinas, S. V., and Liew, S. C.: Tropical cirrus cloud contamination in sun photometer data, Atmos. Environ., 45, 6724–6731, doi:10.1016/j.atmosenv.2011.08.017, 2012. 17305

Dahlkötter, F., Gysel, M., Sauer, D., Minikin, A., Baumann, R., Seifert, P., Ansmann, A., Fromm, M., Voigt, C., and Weinzierl, B.: The Pagami Creek smoke plume after long-range transport to the upper troposphere over Europe – aerosol properties and black carbon mixing state, Atmos. Chem. Phys., 14, 6111–6137, doi:10.5194/acp-14-6111-2014, 2014. 17301

Damoah, R., Spichtinger, N., Forster, C., James, P., Mattis, I., Wandinger, U., Beirle, S., Wagner, T., and Stohl, A.: Around the world in 17 days - hemispheric-scale transport of forest fire smoke from Russia in May 2003, Atmos. Chem. Phys., 4, 1311–1321, doi:10.5194/acp-4-1311-2004, 2004. 17301

Draxler, R. R.: HYSPLIT4 user's guide, NOAA Tech. Memo. ERL ARL-230, NOAA Air Resources Laboratory, Silver Spring, MD, 1999. 17306

Draxler, R. R. and Hess, G. D.: Description of the HYSPLIT 4 modeling system, NOAA Tech. Memo. ERL ARL–224, NOAA Air Resources Laboratory, Silver Spring, MD, 1997. 17306

Draxler, R. R. and Hess, G. D.: An overview of the HYSPLIT 4 modeling system of trajectories, dispersion, and deposition, Aust. Meteorol. Mag., 47, 295–308, 1998. 17306

Fiebig, M., Petzold, A., Wandinger, U., Wendisch, W., Kiemle, C., Stifter, A., Ebert, M., Rother, T., and Leiterer, U.: Method, accuracy, and inferable properties applied to a biomass-burning aerosol and its radiative forcing, J. Geophys. Res., 107, 8130, doi:10.1029/2000JD000192, 2002. 17300, 17301

Flynn, L. P., Wright, R., Garbeil, H., Harris, A. J. L., and Pilger, E.: A global thermal alert using MODIS: initial results from 2000–2001, Advances in Environmental Monitoring and Modeling, 1, 5–36, 2002. 17306

Freudenthaler, V., Esselborn, M., Wiegner, M., Heese, B., Tesche, M., Ansmann, A., Müller, D., Althausen, D., Wirth, M., Fix, A., Ehret, G., Knippertz, P., Toledano, C., Gasteiger, J., Garhammer, M., and Seefeldner, M.: Depolarization ratio profiling at several wavelengths

in pure Saharan dust during SAMUM 2006, Tellus B, 61, 16579, doi:10.1111/j.1600-0889.2008.00396.x, 2009. 17303

Gaudichet, A., Echalar, F., Chatenet, B., Quisefit, J. P., Malingre, G., Cachier, H., Buat-Menard, P., Artaxo, P., and Maenhaut, W.: Trace elements in tropical African savanna biomass burning aerosols, J. Atmos. Chem., 22, 19–39, 1995. 17301

Giglio, L., Descloitres, J., Justice, C. O., and Kaufman, Y. J.: An enhanced contextual fire detection algorithm for MODIS, Remote Sens. Environ., 87, 273–282, 2003. 17306

Groß, S., Tesche, M., Freudenthaler, V., Toledano, C., Wiegner, M., Ansmann, A., Althausen, D., and Seefeldner, M.: Characterization of Saharan dust, marine aerosols and mixtures of biomass-burning aerosols and dust by means of multi-wavelength depolarization and Raman lidar measurements during SAMUM 2, Tellus B, 63, 70624, doi:10.1111/j.1600-0889.2011.00556.x, 2011. 17302, 17304, 17309

Groß, S., Esselborn, M., Weinzierl, B., Wirth, M., Fix, A., and Petzold, A.: Aerosol classification by airborne high spectral resolution lidar observations, Atmos. Chem. Phys., 13, 2487–2505, doi:10.5194/acp-13-2487-2013, 2013. 17302, 17304

Hänel, A., Baars, H., Althausen, D., Ansmann, A., Engelmann, R., and Sun, J. Y.: One-year aerosol profiling with EUCAARI Raman lidar at Shangdianzi GAW station: Beijing plume and seasonal variations, J. Geophys. Res., 117, D13201, doi:10.1029/2012JD017577, 2012. 17309

Holben, B. N., Eck, T. F., Slutsker, I., Tanré, D., Buis, J. P., Setzer, A., Vermote, E., Reagan, J. A., Kaufman, Y. J., Nakajima, T., Lavenu, F., Jankowiak, I., and Smirnov, A.: AERONET – a federated instrument network and data archive for aerosol characterization, Remote Sens. Environ., 66, 1–16, 1998. 17305

Maenhaut, W., Salma, I., Cafmeyer, J., Annegarn, H. J., and Andreae, M. O.: Regional atmospheric aerosol composition and sources in the eastern Transvaal, South Africa, and impact of biomass burning, J. Geophys. Res., 101, 23631–23650, doi:10.1029/95JD02930, 1996. 17301

Mamouri, R. E. and Ansmann, A.: Fine and coarse dust separation with polarization lidar, Atmos. Meas. Tech. Discuss., 7, 5173–5221, doi:10.5194/amtd-7-5173-2014, 2014. 17301, 17304, 17305, 17311, 17327, 17329

Mamouri, R. E., Ansmann, A., Nisantzi, A., Kokkalis, P., Schwarz, A., and Hadjimitsis, D.: Low Arabian dust extinction-to-backscatter ratio, Geophys. Res. Lett., 40, 4762–4766, doi:10.1002/grl.50898, 2013. 17303, 17304, 17305, 17311, 17319

Markham, B. L., Schafer, J. S., Holben, B. N., and Halthore, R. N.: Atmospheric aerosol and water vapor characteristics over north central Canada during BOREAS, J. Geophys. Res., 102, 29737–29745, doi:10.1029/97JD00241, 1997. 17309

Mattis, I., Ansmann, A., Wandinger, U., and Müller, D.: Unexpectedly high aerosol load in the free troposphere over central Europe in spring/summer 2003, Geophys. Res. Lett., 30, 2178, doi:10.1029/2003GL018442, 2003. 17300, 17309

Mattis, I., Müller, D., Ansmann, A., Wandinger, U., Preißler, J., Seifert, P., and Tesche, M.: Ten years of multiwavelength Raman lidar observations of free-tropopsheric aerosol layers over central Europe: geometrical properties and annual cycle, J. Geophys. Res., 113, D20202, doi:10.1029/2007JD009636, 2008. 17301

Müller, D., Mattis, I., Wandinger, U., Ansmann, A., Althausen, A., and Stohl, A.: Raman lidar observations of aged Siberian and Canadian forest fire smoke in the free troposphere over Germany in 2003: microphysical particle characterization, J. Geophys. Res., 110, D17201, doi:10.1029/2004JD005756, 2005. 17301, 17309

Müller, D., Mattis, I., Ansmann, A., Wandinger, U., Ritter, C., and Kaiser, D.: Multiwavelength Raman lidar observations of particle growth during long-range transport of forest-fire smoke in the free troposphere, Geophys. Res. Lett., 34, L05803, doi:10.1029/2006GL027936, 2007. 17309

Murayama, T., Müller, D., Wada, K., Shimizu, A., Sekiguchi, M., and Tsukamoto, T.: Characterization of Asian dust and Siberian smoke with multiwavelength Raman lidar over Tokyo, Japan in spring 2003, Geophys. Res. Lett., 31, L23103, doi:10.1029/2004GL021105, 2004. 17301, 17309

O'Neill, N. T., Eck, T. F., Holben, B. N., Smirnov, A., Royer, A., and Li, Z.: Optical properties of boreal forest fire smoke drived from Sun photometry, J. Geophys. Res., 107, AAC 6-1–AAC 6-19, doi:10.1029/2001JD000877, 2002. 17309

O'Neill, N. T., Eck, T. F., Smirnov, A., Holben, B. N., and Thulasiraman, S.: Spectral discrimination of coarse and fine mode optical depth, J. Geophys. Res., 108, 4559, doi:10.1029/2002JD002975, 2003. 17305

Palmer, T. Y.: Large fire winds, gases and smoke, Atmos. Environ., 15, 2079–2090, 1981. 17301

Pappalardo, G., Amodeo, A., Apituley, A., Comeron, A., Freudenthaler, V., Linné, H., Ansmann, A., Bösenberg, J., D'Amico, G., Mattis, I., Mona, L., Wandinger, U., Amiridis, V., Alados-Arboledas, L., Nicolae, D., and Wiegner, M.: EARLINET: towards an advanced

sustainable European aerosol lidar network, Atmos. Meas. Tech. Discuss., 7, 2929–2980, doi:10.5194/amtd-7-2929-2014, 2014. 17303

Petzold, A., Weinzierl, B., Huntrieser, H., Stohl, A., Real, E., Cozic, J., Fiebig, M., Hendricks, J., Lauer, A., Law, K., Roiger, A., Schlager, H., and Weingartner, E.: Perturbation of the European free troposphere aerosol by North American forest fire plumes during the ICARTT-ITOP experiment in summer 2004, Atmos. Chem. Phys., 7, 5105–5127, doi:10.5194/acp-7-5105-2007, 2007. 17301

Pratt, K. A., Murphy, S. M., Subramanian, R., DeMott, P. J., Kok, G. L., Campos, T., Rogers, D. C., Prenni, A. J., Heymsfield, A. J., Seinfeld, J. H., and Prather, K. A.: Flight-based chemical characterization of biomass burning aerosols within two prescribed burn smoke plumes, Atmos. Chem. Phys., 11, 12549–12565, doi:10.5194/acp-11-12549-2011, 2011. 17301

Sakai, T., Nagai, T., Zaizen, Y., and Mano, Y.: Backscattering linear depolarization ratio measurements of mineral, sea-salt, and ammonium sulfate particles simulated in a laboratory chamber, Appl. Optics, 49, 4441–4449, 2010. 17304

Full Screen / Esc

Printer-friendly Version

Interactive Discussion
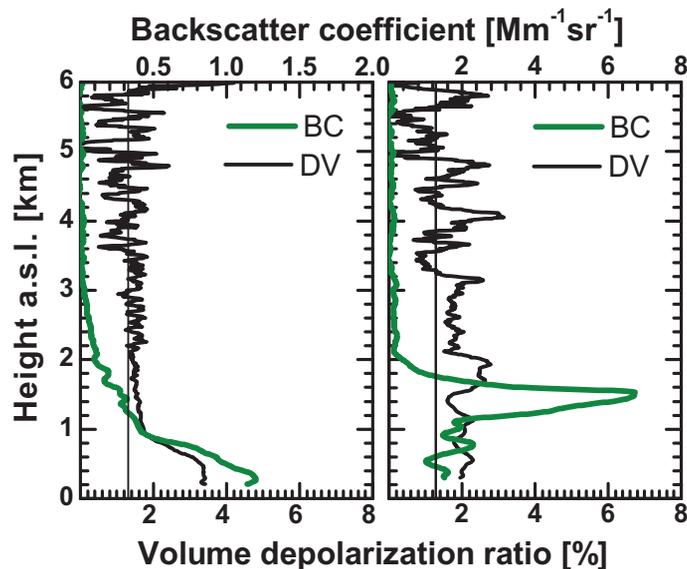
Figure 1. 532 nm particle backscatter coefficient (BC, green) and volume linear depolarization ratio (DV, black) measured on two days with almost particle-free conditions above 2–3 km height. The vertical lines indicate DV = 1.3 %. This value was used in the data analysis as Rayleigh depolarization ratio (clear air DV).

9 Aug 2012, 1030-1130 UTC, smoke-free case

$AE_A = 1.67 \pm 0.03$
$AOT_A = 0.31 \pm 0.03$
$FMF_A = 0.76 \pm 0.02$

$S_{FT} = 37 \, sr$
$S_{PBL} = 29 \, sr$
$S_{COL} = 35 \, sr$
$\delta_{FT} = 6.9 \, \%$

Height a.s.l. [km]

Backscatter coef. [Mm^{-1}sr^{-1}]   Depolarization ratio [%]
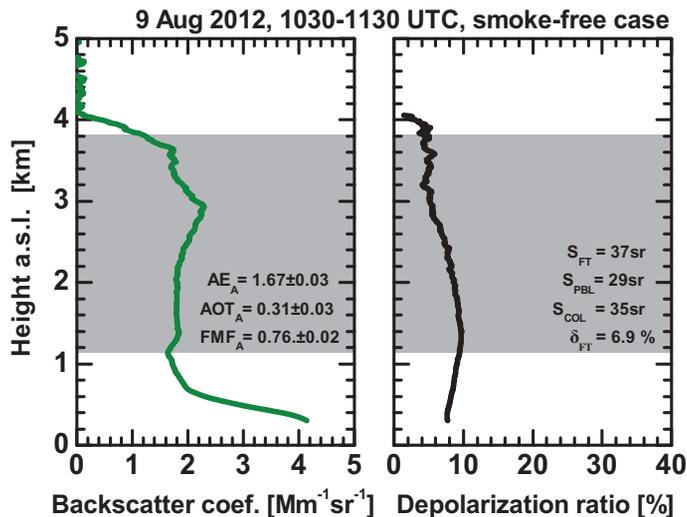
Figure 2. 532 nm particle backscatter coefficient (left, green) and particle linear depolariza-
tion ratio (right, black) in the free troposphere during northerly airflow. No fires occurred over
Turkey (smoke-free case). The grey-shaded area indicates the identified lofted aerosol layer.
AE_A, AOT_A, and FMF_A in the left panel denote Ångström exponent, particle optical depth, and
fine-mode fraction derived from AERONET photometer observations (for the total tropospheric
column). Retrieved lidar ratios S_{FT} for the free troposphere and S_{COL} for the total column, ob-
tained after Mamouri et al. (2013) by assuming the boundary layer lidar ratio S_{PBL} (for the lowest
400 m) are given in the right panel. In addition, the mean particle depolarization ratio δ_{FT} for
the grey–shaded lofted aerosol layer is given.
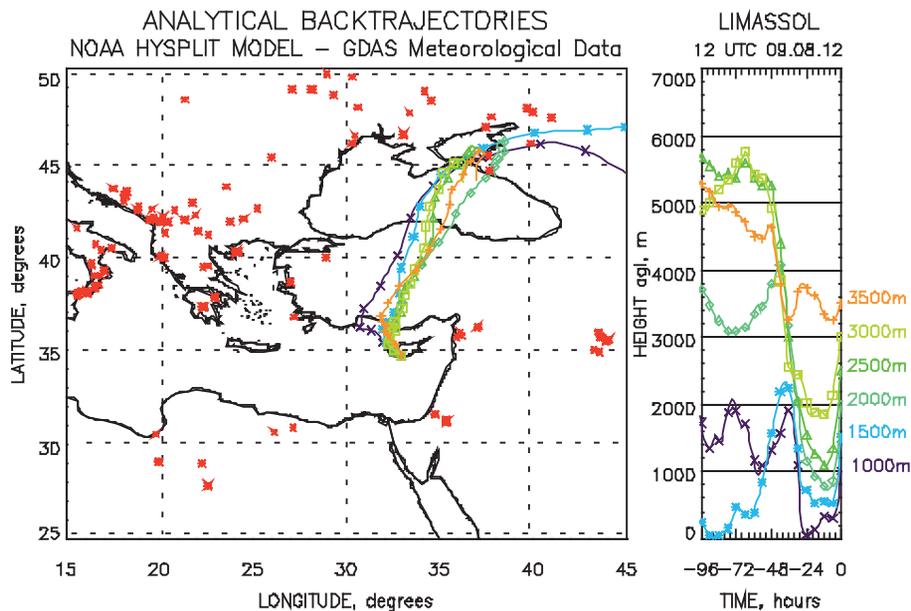
Figure 3. Four-day HYSPLIT backward trajectories arriving at Limassol, Cyprus, at different height levels (blue, green, orange) on 9 August 2012, 12:00 UTC. Red crosses indicate fire events which occurred during the time period from 4–9 August 2012 according to MODIS observations.
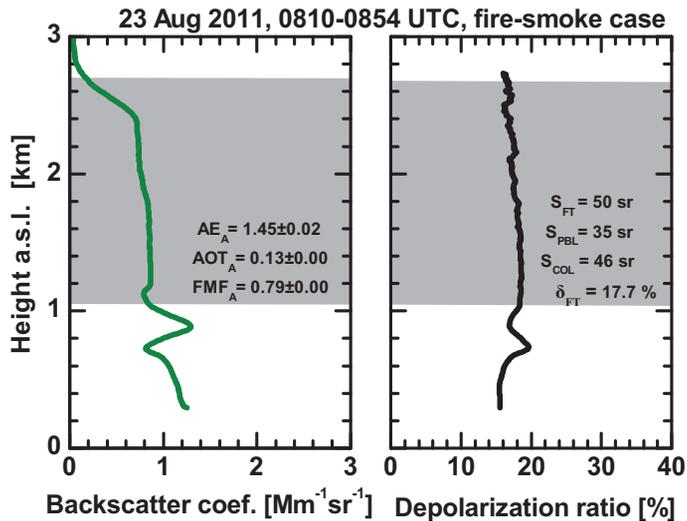
Figure 4. Same as Fig. 2, except for 23 August 2011. A fire smoke case is shown, i.e., air masses crossed fire areas over Turkey before reaching the lidar site.
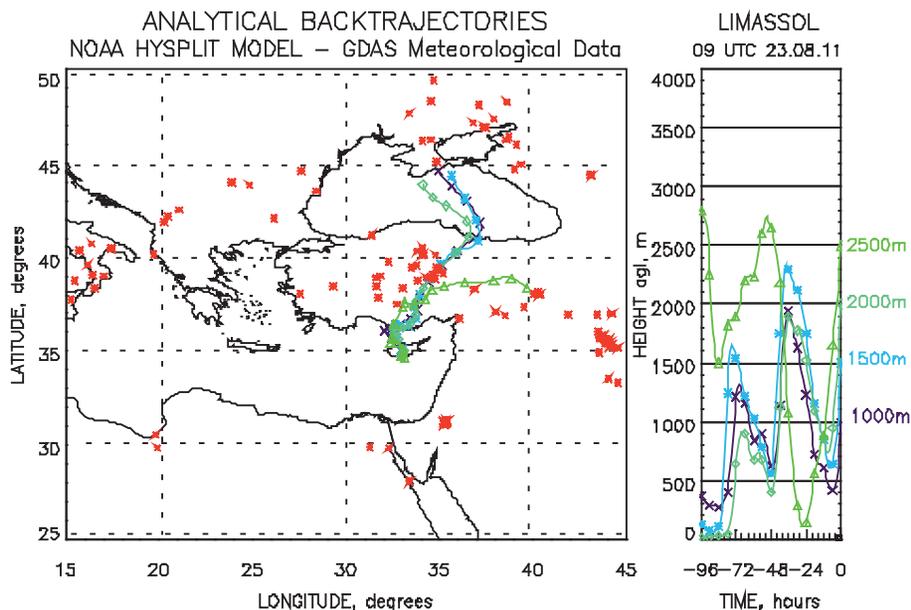
Figure 5. Same as Fig. 3, except for 23 August 2011. Red crosses indicate fire events which occurred during the time period from 18–23 August 2012.

Full Screen / Esc

Printer-friendly Version

Interactive Discussion
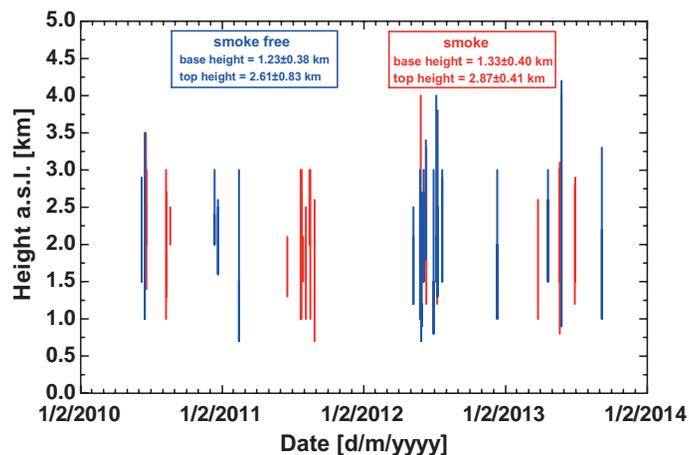
Figure 6. Lofted free-tropospheric aerosol layers (shown as vertical lines from bottom to top) observed during northerly air flows between April 2010 and February 2014. In the case of the blue vertical lines (21 smoke-free cases) no fire events over Turkey occured and influenced the lidar measurements. In the case of the red layers (24 fire smoke cases), the air masses crossed fire areas over Turkey before arriving at the lidar site at Limassol. The average bottom and top heights (plus one standard deviation) of all detected layers, separately for smoke and smoke-free cases, are given in addition.
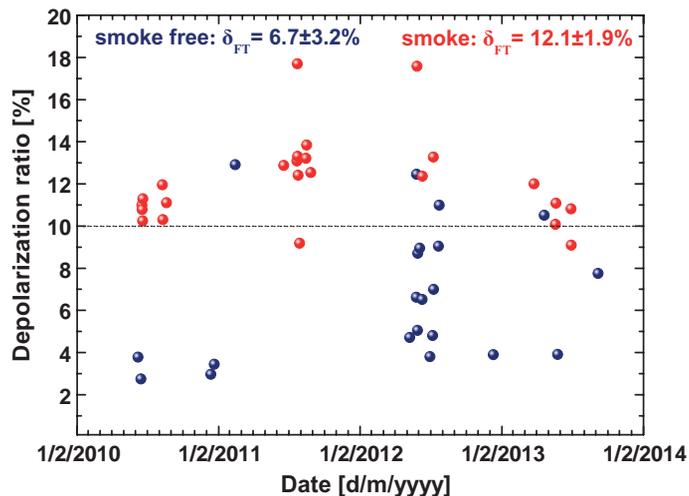
Figure 7. Layer-mean particle depolarization ratio of all 21 blue layers (no influence of Turkish smoke) and 24 red layers (influenced by fires in Turkey) that are given in Fig. 6. Most fire-smoke cases show enhanced particle depolarization ratios (> 10 %, red circles). The average layer-mean depolarization ratios of all 21 blue and 24 red layers and corresponding standard deviations are given as numbers.

Full Screen / Esc
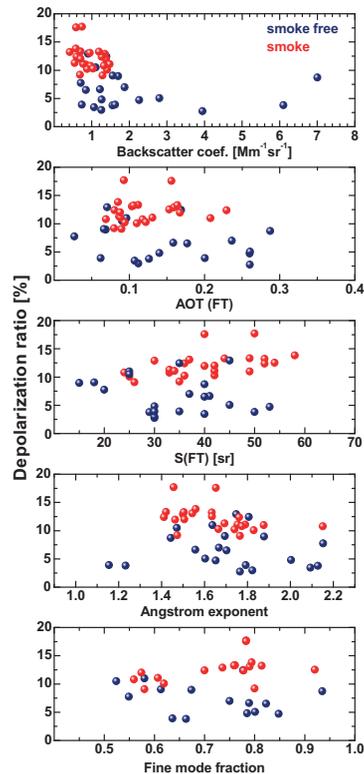
Figure 8. Range of observed values of the particle backscatter coefficient (mean value of the lofted aerosol layers), free-tropospheric aerosol particle optical thickness AOT(FT), lidar ratio S(FT) in the lofted aerosol layers, Ångström exponent for the total vertical column, and fine mode fraction (regarding the total tropospheric 500 nm AOT) for the Turkish fire-smoke cases (red circles) and the cases without smoke from Turkey (blue circles). All values (circles) are given as a function of layer-mean particle depolarization ratio to better distinguish between fire-smoke and smoke-free cases.
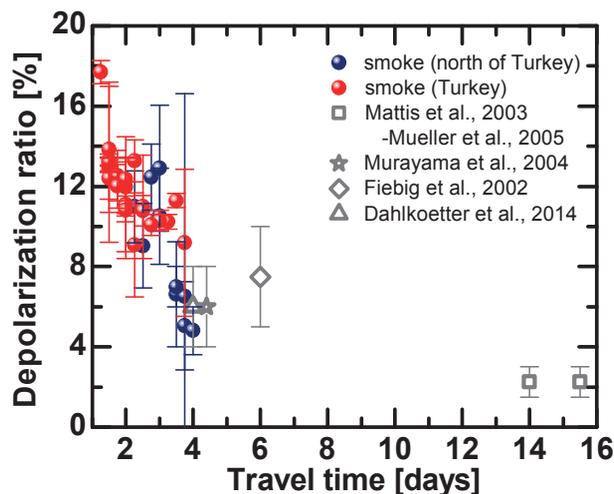
Figure 9. Decrease of the layer-mean particle depolarization ratio of smoke-influenced aerosol layers with increasing travel time, defined as the temporal distance between Limassol and the last fire area which the observed air masses crossed before arriving at Limassol. Ten of the 21 blue circles (cases without Turkish smoke) were influenced by smoke generated in areas north of the Black Sea. Grey symbols show observations as published in the given literature. Vertical bars show the range of observed depolarization ratios (literature values) or show the standard deviation of the all values determined within the individual layers (red and blue values).
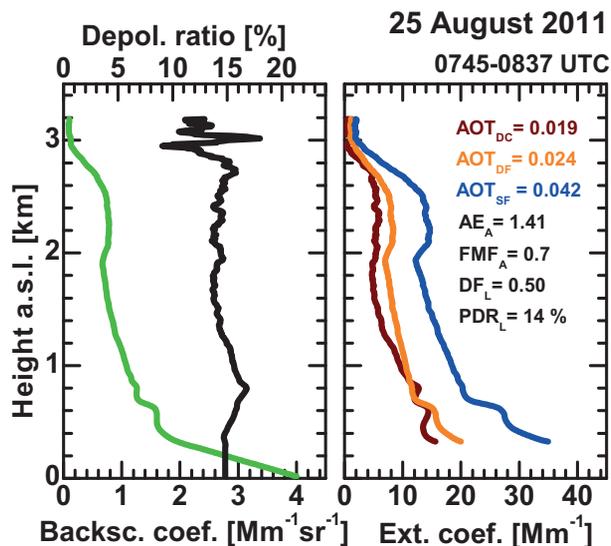
Figure 10. 532 nm particle backscatter coefficient (green profile, left panel), particle linear depolarization ratio (black profile, left panel), and lidar-derived particle extinction coefficients (right panel) for spherical fine-mode particles (blue profile, index SF), fine-mode dust particles (orange profile, index DF), and coarse-mode dust particles (dark red profile, index DC). The extinction coefficient profiles are obtained by using the method of Mamouri and Ansmann (2014). The respective free tropospheric AOTs (above 300–400 m height), the AERONET–derived Ångström exponent AE_A and fine-mode fraction FMF_A (for total tropospheric column), and the lidar-derived dust fraction DF_L (with respect to the free tropospheric 532 nm AOT) are given as numbers together with the layer-mean depolarization ratio PDR_L. The measurement was taken on 25 August 2011.
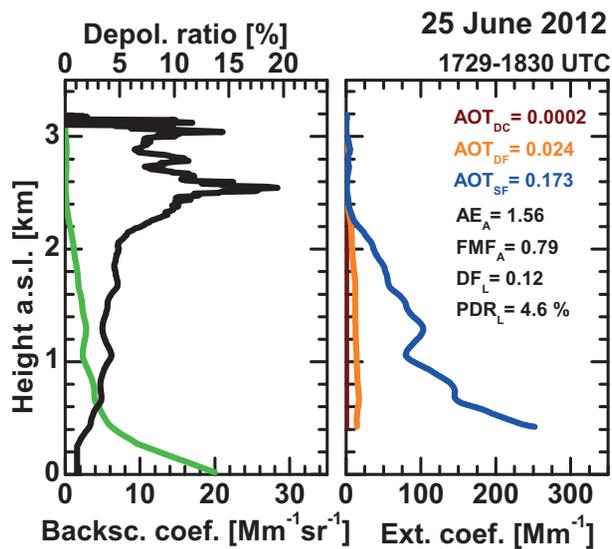
Figure 11. Same as Fig. 10, except for 25 June 2012.

Title Page

Abstract | Introduction

Conclusions | References

Tables | Figures

|◄ | ►|

◄ | ►

Back | Close

Full Screen / Esc

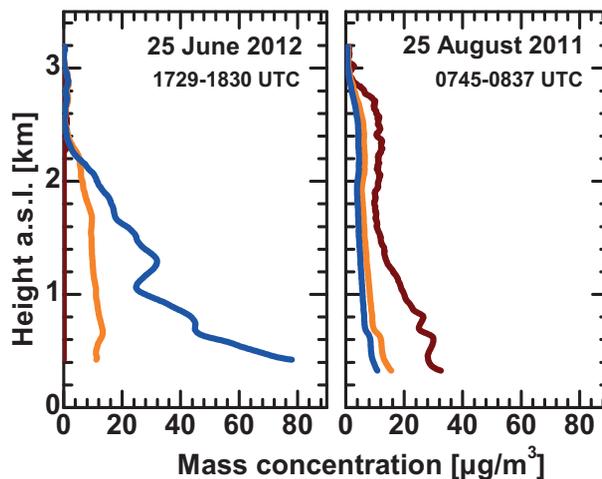Printer-friendly Version

Interactive Discussion

Figure 12. Particle mass concentration profiles (blue: spherical fine-mode particles, orange: fine-mode dust, dark red: coarse-mode dust) estimated from the particle extinction profiles in Figs. 10 and 11 after the method of Ansmann et al. (2012). Fine-mode and coarse-mode dust mass retrieval is described by Mamouri and Ansmann (2014).